Quantifying and predicting near-wall global intermittency in stably stratified channel flow

Haoyang Cen, Artem Korobenko [ORCID], and Qi Zhou [ORCID][*]
Schulich School of Engineering, University of Calgary, Calgary, AB T2N 1N4, Canada

In this study we investigate stably stratified channel flow (SCF) between two solid walls, focusing on its transition from fully developed turbulence to the onset of global intermittency, characterized by the coexistence of laminar and turbulent patches in the flow. With direct numerical simulations, we examine this transition across various friction Reynolds ($180 < \text{Re}_\tau < 960$) and shear Richardson ($\text{Ri}_\tau$) numbers, parameters that are observed to impact intermittency dynamics. To quantify intermittency, we measure the volume fraction of turbulent patches using enstrophy as a criterion and examine the variation of the turbulent fraction along the wall-normal direction. Our findings reveal that intermittency in SCF can originate independently from either near-wall or midchannel regions, depending on the values of Re_τ and Ri_τ. With increased stratification, intermittency originating from both regions may merge across the channel's depth. Particular attention is paid to near-wall intermittency (NWI) and identifying its occurrence boundary within the Re_τ-Ri_τ parameter space. We assess various dimensionless parameters for their ability to predict NWI, discovering that intermittency consistently occurs when the Nusselt number falls below a critical value of approximately 3.0. To establish the intermittency boundary following this Nusselt number criterion, a Reynolds-averaged Navier-Stokes model is formulated based on a first-order closure scheme. This model proves effective in predicting the occurrence of NWI in SCF in terms of Re_τ and Ri_τ. Furthermore, we verify the Nu scaling recently proposed by Zonta *et al.* [J. Fluid Mech. **945**, A3 (2022)], which leads to an intermittency boundary in the form of $\text{Re}_\tau^2 \text{Ri}_\tau^{-1} = \text{const}$.

I. INTRODUCTION

Global intermittency, as defined by Mahrt [1], refers to the uneven distribution (or "pathiness") of turbulence on a scale larger than the "main eddies." In contrast, small-scale intermittency concerns the substructure of the main eddies and is characterized by rapid local fluctuations in turbulence properties, such as dissipation [2,3]. In stably stratified atmospheric boundary layers during the nocturnal cycle, when significant surface cooling occurs at the ground, a stationary observer would detect globally intermittent flows as episodes of intense turbulence interspersed with periods of weak fluctuations [4–6]. Numerical studies of stably stratified flows demonstrate global intermittency through the simultaneous coexistence of laminar and turbulent patches within the flow [7–11].

In the context of stable atmospheric boundary layers, global intermittency (hereinafter referred to as "intermittency" for simplicity) is thought to be a result of suppression of turbulence by stratification, with the onset of intermittency often linked to turbulence collapse [7,9]. However, intermittently turbulent states can also occur independently of stratification, such as in nonstratified plane Couette flow experiments with moderate Reynolds numbers [12], which seems to attribute

---

[*]Corresponding author: qi.zhou1@ucalgary.ca

intermittency also to viscous effects. Despite its implications for geophysical flows, our ability to predict the onset of intermittency in stratified wall-bounded turbulence is limited, with the notable exception of Ref. [10], which identified such a boundary for stratified plane Couette flow based on external flow parameters. In the present study, our main goal is to expand this predictive capacity to a different flow configuration, i.e., stably stratified channel flow.

In their study on stratified plane Couette flow (SPCF), Deusebio *et al.* [10] examined the characteristics of intermittency in this wall-bounded flow and highlighted the effects of both stratification and viscosity on the intermittency. They noted qualitative differences in the intermittency at various Reynolds numbers and reported the quantitative effects of a dimensionless parameter, $L^+ \equiv L/\delta_\nu$, on the intermittency. Here L^+ represents the ratio between two length scales: L is the Obukhov length, determined jointly by the wall fluxes of momentum and heat, and δ_ν is the viscous scale at the wall. Based on their direct numerical simulation (DNS) of statistically stationary SPCF, Deusebio *et al.* [10] discovered an increasing trend of the volumetric fraction of turbulence with L^+ for $L^+ < 200$. No intermittency was observed for $L^+ > 200$, leading the authors to propose $L^+ \lesssim 200$ as a criterion for the onset of intermittency. Furthermore, they developed a Reynolds-averaged Navier-Stokes (RANS) model for SPCF, which allowed them to predict L^+ as a function of external flow parameters, such as the bulk Reynolds and Richardson numbers. By combining the RANS model with the $L^+ \lesssim 200$ criterion, Deusebio *et al.* [10] successfully delineated the occurrence boundary for intermittency within the Reynolds-Richardson number parameter space. In the very recent work by Issaev *et al.* [11], a "local" version of L^+ was defined [see their Eq. (3.8)] based on the local Reynolds stress in the interior of an open-channel flow. It was observed that intermittency occurs when the local L^+ falls below 260.

In the present study, we aim to extend the efforts in predicting the onset of intermittency to stratified channel flow (SCF), which exhibits distinct dynamical differences compared to SPCF or stratified open-channel flow. Unlike Couette flow, which is driven purely by shear with zero mean flow when averaged between the two walls, SCF is driven by a pressure gradient and possesses a net mean flow, distinguishing it significantly from Couette flow. The Couette flow is generated by the shearing of two parallel plates moving in opposite directions, leading to a constant-flux layer for both momentum and buoyancy in a statistically stationary state. The concept of a constant-flux layer is fundamental to the formulation of Monin-Obukhov similarity theory but may apply only to the surface layer in a "weakly stable" atmospheric boundary layer (see Fig. 1 of Zhou *et al.* [13] for a schematic illustrating these differences). In both SCF and SPCF, stable stratification is observed extending to the bottom boundary, as noted in various studies such as those by García-Villalba and del Álamo [14] and Deusebio *et al.* [10]. However, in the case of open-channel flow, like the one described by Issaev *et al.* [11], an adiabatic boundary condition is typically set, leading to minimal stratification near the wall. These distinguishing features of SCF, which are not found in previously studied flows, motivate us to focus on SCF in this paper.

To the best of our knowledge, the $L^+ \lesssim 200$ criterion proposed in Ref. [10] has not been validated to be applicable for situations other than a constant-flux layer, which partially motivates our investigation. SCF is characterized by a hot stationary wall at the top and a cold one at the bottom, with a horizontal pressure gradient as the driving force. In fully developed SCF, the turbulent momentum flux or Reynolds stress peaks in the near-wall region (e.g., see Fig. 20 in Ref. [14]) and decreases linearly towards the channel midplane. Due to symmetry, the momentum flux in SCF must vanish at the midplane between the top and bottom walls. The buoyancy flux also exhibits nontrivial variations in the wall-normal direction. These flux variations in SCF make it an appropriate configuration for studying intermittency in non-constant-flux, wall-bounded, stratified shear flows.

SCF has been widely investigated through numerous numerical studies [14–21]. Reference [15] examined SCF at a friction Reynolds number (Re_τ) of 180 using wall-resolved large-eddy simulation. Depending on the relative dominance of stratification and shear, three flow regimes were identified: buoyancy-affected (characterized by general turbulence suppression), buoyancy-controlled (characterized by transient and partial flow relaminarization), and buoyancy-dominated

(characterized by complete flow relaminarization). The condition for flow relaminarization was investigated by Refs. [14,16,17], which reported the sensitivity of the relaminization process to the friction Richardson number, Ri_τ, as well as the size of the computational domain [14]. Such a relaminarization process was interpreted in the framework of the linear stability analysis of a plane Poiseuille flow [22], yielding a "relaminarization boundary" in the Re_τ-Ri_τ plane (e.g., see Fig. 3 of Ref. [14]), i.e., the transition between fully laminarized and intermittently turbulent flows. It is worth noting that in the present study we aim to delineate a different boundary, i.e., the "intermittency boundary," which is between fully turbulent flow and the onset of intermittency. More recent simulations reported in Ref. [20] expanded the Re_τ value to 1000. The authors highlighted the dynamical role of "nonturbulent wavy structures," presumably internal gravity waves, in reducing the wall-normal fluxes of momentum and buoyancy by imposing a "blockage effect" on the interactions between the two walls.

Several flow parameters are considered relevant for maintaining wall-bounded, stratified shear turbulence. The renowned Miles-Howard theorem [23,24] establishes the linear stability of inviscid, parallel shear flow, depending on a critical value of the local gradient Richardson number (Ri_g) of 1/4. Another stability parameter is the length scale ratio, h/L, where h represents a characteristic height of the flow, and L is the Obukhov length. Nieuwstadt [25] presented DNS data that indicated the possibility of relaminarization in open-channel flows subjected to strong cooling at the bottom wall. In this flow the upper boundary condition is characterized by free slip rather than no slip, the latter of which is the condition explored in the current paper. Intermittency occurs when $h/L \gtrsim 1.25$, with h being the height of the open channel. Flores and Riley [7] reported a critical value for h/L of approximately 1.0 for the onset of intermittency also in stratified open-channel flows. However, the h/L criterion was unsuccessful in predicting intermittency for stratified plane Couette flow, as documented in Ref. [10]. Instead, Deusebio *et al.* [10] proposed a criterion of $L^+ \lesssim 200$, which turned out to be effective for the specific flow, a constant-flux layer. This L^+ criterion was adapted by Ref. [11] for stratified open-channel flow. In summary, the criterion for the onset of intermittency in stratified wall-bounded flows remains inconclusive in the literature.

In the broader scope of stably stratified, wall-bounded atmospheric flows, the phenomenon of intermittency plays a crucial role, significantly impacting surface mixing events and turbulence statistics. This is extensively reviewed in the work by Mahrt [2]. A fundamental, yet unresolved, question raised by Mahrt [2] concerns the origin of atmospheric flow intermittency: is it a result of external forces, specifically submeso-scale motions which are typically under 2 km in terms of horizontal scale [2]? Our problem setup, which excludes sophisticated forcing representative of the submeso-scale motions, could shed light on this matter.

The aim of this study is thus to investigate the transition from fully developed turbulence to the onset of intermittency in stably stratified channel flow between two solid walls, focusing specifically on the near-wall region (in contrast to a recent work [11] which focused instead on predicting intermittency throughout the depth in an open-chanel flow). We will utilize our DNS data to characterize intermittency in SCF across a broad range of friction Reynolds and Richardson numbers (Re_τ and Ri_τ), both qualitatively and quantitatively. Additionally, following a similar approach to Deusebio *et al.* [10], we will employ RANS to establish the intermittency boundary in terms of the control parameters.

The remainder of the paper is organized as follows: Sec. II details our numerical simulations. In Sec. III we provide an overview of the qualitative features of intermittency observed in our DNS and some statistics. Section IV focuses on quantifying intermittency in SCF, specifically examining the turbulent volume fraction and its variation along the wall-normal direction. In Sec. V we assess the applicability of various criteria for identifying the onset of intermittency. The Appendix presents the development of a first-order closure model to predict the boundary between fully turbulent and intermittent turbulence in the Re_τ-Ri_τ parameter space, which is shown in Sec. VI. Finally, we offer concluding remarks in Sec. VII.
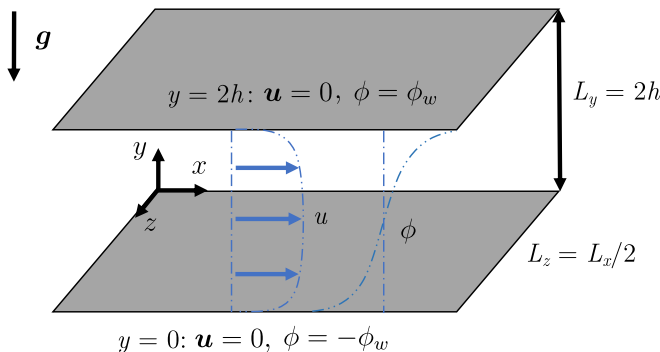
FIG. 1. Schematic illustrating the setup of stratified channel flow along with the respective boundary conditions applied at the top and bottom walls. The computational domain is of the size $L_x \times L_y \times L_z$ represented by $N_x \times N_y \times N_z$ grid points.

II. NUMERICAL SIMULATIONS

In the present study, we examine stratified channel flow in a Cartesian coordinate system $\boldsymbol{x} = (x, y, z)$. The domain is bounded in the vertical (y) direction by two no-slip, impermeable walls separated by a distance of $2h$. The channel flow is driven by a constant mean pressure gradient $\boldsymbol{f} = (u_\tau^2/h, 0, 0)$ in the streamwise (x) direction. Here u_τ is the friction velocity and is related to the wall shear stress that counters the pressure gradient. Numerical periodicity is imposed in the horizontal directions, which are thus considered statistically homogeneous. Stable density stratification is maintained by prescribing a constant potential temperature difference, $\Delta\phi \equiv 2\phi_w$, between the lower (colder) and upper (hotter) walls. A schematic diagram of the configuration and boundary conditions for SCF is presented in Fig. 1. It is important to distinguish the current setup of SCF with stratified open-channel flow, where the top wall is absent, a flow that has been the subject of other studies [7,11,25–27].

The fluid dynamics of SCF are described by the Navier-Stokes equations for incompressible flows under the Boussinesq approximation, as follows:

$$\nabla \cdot \boldsymbol{u} = 0, \tag{1a}$$

$$\frac{\partial \boldsymbol{u}}{\partial t} + \boldsymbol{u} \cdot \nabla \boldsymbol{u} = -\frac{\nabla p}{\rho_0} + \nu\nabla^2\boldsymbol{u} + \boldsymbol{f} + \alpha_V \phi\boldsymbol{g}, \tag{1b}$$

where $\boldsymbol{u} = (u, v, w)$ represents the fluid velocity, ρ_0 denotes the reference density, ϕ stands for the potential temperature, $\boldsymbol{g} \equiv -g\boldsymbol{e}_y$ signifies the gravitational force acting in the y direction with g being the gravitational constant, α_V is the thermal expansion coefficient in the linear equation of state, and ν refers to the kinematic viscosity. The evolution of the potential temperature, ϕ, is described by the advection–diffusion equation as follows:

$$\frac{\partial \phi}{\partial t} + \boldsymbol{u} \cdot \nabla \phi = \kappa\nabla^2\phi, \tag{2}$$

with κ being the thermal diffusivity. In the present study, the Prandtl number $\mathrm{Pr} = \nu/\kappa$ is set to 0.71 to model thermal stratification in air.

Two dimensionless parameters can be defined based on dynamical quantities at the walls, i.e., the friction Reynolds number,

$$\mathrm{Re}_\tau \equiv \frac{u_\tau h}{\nu}, \tag{3}$$

and the shear (friction) Richardson number [15],

$$\mathrm{Ri}_\tau \equiv \frac{2\phi_w \alpha_V g h}{u_\tau^2}. \tag{4}$$

In these equations $u_\tau \equiv \sqrt{\nu(\partial U/\partial y)_w}$ relates the friction velocity to the gradient of the mean streamwise velocity at the walls, $(\partial U/\partial y)_w$. Here and throughout the paper, the subscript w denotes values evaluated at the walls, and $U \equiv \langle u \rangle$ is the mean streamwise velocity with $\langle \cdot \rangle$ denoting horizontal averages over the statistically homogeneous x-z plane. Similarly, the mean potential temperature is denoted as $\Phi \equiv \langle \phi \rangle$. In a statistically stationary turbulent state, the wall shear in the current setting must compensate for the applied streamwise pressure gradient f to maintain momentum balance in the system.

The governing equations, Eqs. (1) and (2), are solved using direct numerical simulation (DNS). Comprehensive descriptions of the DNS algorithm can be found in Ref. [28]. The DNS algorithm has been extensively validated and employed to study wall-bounded turbulent flows (see, e.g., Refs. [10,13,29]), including the work by Deusebio *et al.* [10]. Spectral Fourier modes are utilized for spatial discretization in the horizontal (x and z) directions, while the wall-normal (y) direction is discretized using a second-order finite difference method. The convective terms are advanced in time through a low-storage third-order Runge-Kutta method, while the viscous and diffusive terms at each time step are updated using a semi-implicit Crank-Nicolson method. The convective terms are evaluated in physical space, with a two-thirds dealiasing rule applied to the two horizontal directions to prevent aliasing errors [30]. Adaptive time stepping, based on a Courant-Friedrichs-Lewy number of 0.5, is enabled to reduce computational time while maintaining numerical stability.

Following standard practices for DNS of wall-bounded turbulent flows [31], we utilize uniform grids for the horizontal directions with spacings of $\Delta x^+ \simeq 8$ and $\Delta z^+ \simeq 4$. The superscript $+$ denotes nondimensionalized quantities with respect to the near-wall viscous length scale $\delta_\nu = \nu/u_\tau$. In the wall-normal direction y, the grid is condensed towards the walls using a hyperbolic tangent stretching function, which provides better resolution of small-scale structures in the near-wall region. In this study we investigate SCF for a range of Re_τ. For each Re_τ, the grid is adjusted such that the distance of the tenth point to the wall satisfies $y_{10}^+ < 10$ (see, e.g., Ref. [31]), following DNS of stratified wall-bounded turbulent flows using the same solver [10,29]. As Re_τ increases, the required grid spacing for resolving the smallest turbulent length scales decreases, necessitating more grid points. Consequently, the computational cost increases rapidly with Re_τ. To maintain an affordable cost, the computational domain in the present study is adjusted for each Re_τ, with the smallest ones (for cases with $\mathrm{Re}_\tau = 480$ and 960 as shown in Table I) sized at $L_x \approx 6000\delta_\nu$ and $L_z \approx 3000\delta_\nu$. Such a size is large enough to accommodate more than 900 minimal flow units; each of the minimal flow units is approximately 200 and 100 wall units long in x and z directions, respectively [32].

The size of the computational domain has been reported to play a crucial role in successful numerical simulations of SCF. SCF may undergo nonphysical laminarization in computational domains that can barely contain one minimal flow unit [32,33]. Another indication of domain confinement, according to Ref. [14], is low-frequency oscillations with a period of $O(10u_\tau/h)$ in the temporal evolution of bulk quantities. In the present study, all simulations maintain either fully or intermittently turbulent conditions at a statistically stationary state with no significant flow-frequency oscillation in the temporal statistics, suggesting robust turbulence free of finite-domain effects in our simulations. Some examples of the temporal statistics can be found in Fig. 4.2 of Ref. [21].

In this study we consider SCF at four values of Re_τ ranging from 180 to 960, as shown in Table I where a summary of simulation parameters and grid resolution is provided. At each Re_τ, several degrees of stratification are imposed. The stratification level is varied incrementally from moderate to relatively strong, leading the flows to transition from fully turbulent to intermittent, as suggested by the decreasing values of γ_w, the near-wall turbulent fraction (to be defined in Sec. IV),

TABLE I. Summary of simulation parameters and grid resolution. The last column shows the value of the turbulent fraction at the wall, γ_w, which is discussed in Sec. IV.

Case	Re_τ	Ri_τ	Re	Nu	$(L_x, L_z)/h$	(N_x, N_y, N_z)	L^+	h/L	γ_w
1		18	3044	4.10			1554	0.12	1.00
2		36	3217	3.32			957	0.19	1.00
3	180	60	3464	2.83	$(16\pi, 8\pi)$	$(1024, 129, 1024)$	670	0.27	0.80
4		80	3579	2.62			548	0.33	0.68
5		120	3856	2.33			408	0.44	0.57
6		72	7108	4.70			1360	0.26	1.0
7		140	7652	3.75			875	0.41	1.0
8	360	280	8651	3.07	$(8\pi, 4\pi)$	$(1024, 161, 1024)$	523	0.68	1.0
9		560	10 313	2.46			335	1.07	0.83
10		840	11 753	2.23			247	1.46	0.71
11		500	13 070	3.12			551	0.88	1.0
12		800	15 004	2.85			394	1.25	0.91
13	480	1000	15 977	2.56	$(4\pi, 2\pi)$	$(768, 289, 768)$	277	1.75	0.83
14		1200	17 239	2.41			261	1.84	0.78
15		1600	18 812	2.23			246	1.96	0.74
16	960	2000	40 026	4.26	$(2\pi, \pi)$	$(768, 385, 768)$	415	2.36	1.0
17		3840	46 432	2.76			309	3.10	0.86

with increasing Ri_τ. In the present study, the runs with the lowest values of Ri_τ are initialized from the neutral (nonstratified) statistically stationary states of the corresponding Re_τ. Runs with stronger stratification are each initialized from the statistically stationary state of the previous run (at the immediate lower Ri_τ). The Ri_τ value is adjusted from one simulation to another by changing the product $g\alpha_V$ in Eq. (4), and Re_τ is varied by adjusting the viscosity. The lightest run in the present study (Case 1 in Table I) takes roughly 6000 core hours, while the heaviest (Case 17) takes more than 500 000 core hours. The substantial increase in computation is mainly attributed to the significantly smaller time step required to maintain numerical stability. In the following discussion, a particular case is referred to according to its friction Reynolds and Richardson numbers for ease of reference. For example, the case with $(\mathrm{Re}_\tau, \mathrm{Ri}_\tau) = (360, 560)$ is denoted as Re360-Ri560 (with the subscript τ dropped). As Re_τ and Ri_τ vary from one simulation to another, the flow's bulk Reynolds number, Re, and Nusselt number, Nu, also vary accordingly. The bulk Re is defined in terms of the volume-averaged (bulk) streamwise velocity, u_b, in the channel,

$$\mathrm{Re} \equiv \frac{u_b h}{\nu}, \tag{5}$$

while Nu is associated with the convective heat transfer coefficient $\mathcal{H}$, the characteristic length $\mathcal{L}$, and the thermal conductivity κ, in the following form:

$$\mathrm{Nu} \equiv \frac{\mathcal{H}\mathcal{L}}{\kappa}. \tag{6}$$

Here $\mathcal{H}$ is the ratio between the heat flux q and the temperature difference between the two solid walls, $2\phi_w$, i.e., $\mathcal{H} = q/(2\phi_w)$, and $\mathcal{L}$ can be taken as the channel height, $2h$ (see Fig. 1). The heat flux across the flow can be calculated based on the mean temperature gradient at the wall, $(\partial\Phi/\partial y)_w$, i.e., $q = \kappa(\partial\Phi/\partial y)_w$. Therefore,

$$\mathrm{Nu} = \frac{\kappa\left(\dfrac{\partial\Phi}{\partial y}\right)_w}{2\phi_w} 2h \frac{1}{\kappa} = \frac{\left(\dfrac{\partial\Phi}{\partial y}\right)_w}{\dfrac{\phi_w}{h}}. \tag{7}$$

The Nusselt number (Nu) can be interpreted as the ratio of these two heat transfer scenarios. It compares the actual heat transfer due to convection in the fluid to what the heat transfer would be under the hypothetical scenario where all heat transfer is through pure conduction (e.g., when the fluid is motionless). This ratio Nu measures the enhancement of heat transfer due to the fluid's motion, i.e., higher Nu would imply that convection plays a significant role in heat transfer, making the process more efficient than it would be in a purely conductive scenario. This physical implication of Nu as it relates to the prediction of intermittency will be revisited in Sec. V.

III. FLOW CHARACTERISTICS

A. Phenomenology of intermittency

First, a qualitative understanding of intermittency at various flow parameters can be obtained through flow visualization. Figure 2 displays selected snapshots of streamwise velocity fluctuations, $u' = u - U$, on distinct horizontal (x-z) planes for cases of low and intermediate Re_τ values, specifically for cases Re180-Ri120 and Re480-Ri500. These snapshots are taken during the statistically stationary phase of the flow. In the Re180-Ri120 case, laminar patches can be seen across the channel depths, akin to those observed in Ref. [14]. Although fine-scale turbulence occupies a considerable portion of the near-wall region [Fig. 2(a); $y^+ = 15$], streaky structures characteristic of near-wall turbulence disappear at midchannel [Fig. 2(g); $y^+ = 180$].

The Re480-Ri500 case exhibits qualitative differences when compared to the Re180-Ri120 case. With a larger Ri_τ of 500, the flow at midchannel ($y^+ = 480$) is almost entirely laminar, with only a small portion of the domain displaying noticeable turbulent fluctuations [Fig. 2(h)]. Nevertheless, the larger Re_τ of 480 allows near-wall turbulence to remain robust enough to counterbalance the suppression caused by stratification. As shown in Figs. 2(b) and 2(d), which focus on $y^+ = 15$ and 240 respectively, turbulence retains consistent intensity across the entire x-z plane, with no apparent intermittency. As the distance from the wall increases, intermittency begins to appear, as indicated by the partial laminarization at $y^+ = 384$ [Fig. 2(f)] and the nearly total laminarization at $y^+ = 480$. A comparison of the two columns in Fig. 2 implies that intermittency may either persist throughout the entire channel depth or be partially present in the midchannel region.

B. One-point statistics

Here we probe the flow further using one-point statistics. Figure 3 displays the mean streamwise velocity (U) and potential temperature (Φ) profiles for simulations with $\mathrm{Re}_\tau = 180$ and 480 at increasing levels of stratification, represented by larger Ri_τ values. As stratification increases for a given Re_τ, there is a notable increase in bulk flow velocity, as illustrated in Figs. 3(a) and 3(b). By maintaining a consistent pressure gradient and diminishing turbulence through stratification, the flow indeed encounters smaller frictional losses, leading to acceleration, and thus an increase in the kinetic energy in the system. Consequently, the bulk Reynolds number Re of the flow also increases (see Table I). Despite the increased Ri_τ, the wall shear and the gradient of the mean streamwise velocity at the wall, $(\partial U / \partial y)_w$, remain constant due to the constant pressure gradient, u_τ^2 / h, under the same value of Re_τ.

The value of Ri_τ also has a significant impact on the mean potential temperature, as illustrated in Figs. 3(c) and 3(d). First, the heat flux and the gradient of the potential temperature at the wall decrease as Ri_τ increases, resulting in a reduced Nusselt number, as shown in Table I. Second, the potential temperature profile exhibits a steeper gradient near the channel's midplane ($y/h = 1$), indicating a tendency to form a density interface therein. It is important to note that, unlike in plane Couette flow, where a constant flux layer exists in the midgap region [10,29], the vertical momentum transport ceases in SCF as the channel's core is approached due to the symmetry of the flow configuration.

The wall-normal profiles of the plane-averaged fluctuation kinetic energy (FKE), $k = \langle u'u' + v'v' + w'w' \rangle / 2$, are displayed in Figs. 4(a) and 4(b) for cases with $\mathrm{Re}_\tau = 180$ and 480, respectively.
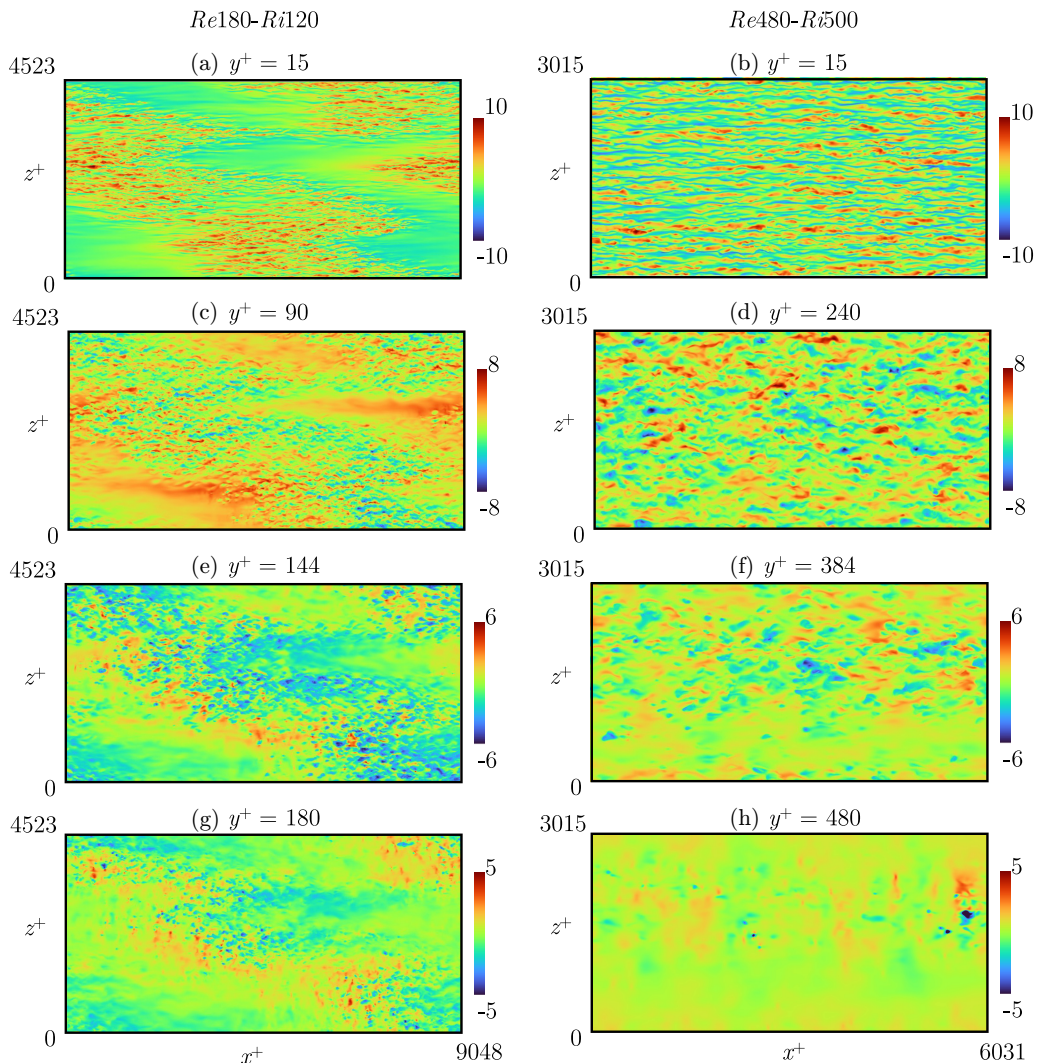
FIG. 2. Sample horizontal transects depicting the instantaneous streamwise velocity fluctuation, u', normalized by the friction velocity, u_τ, for two cases: Re180-Ri120 (left column) and Re480-Ri500 (right column).

In both groups, the profiles reach their peaks in the near-wall region. It is somewhat counterintuitive that k, after being normalized by u_τ^2 (which remains constant for all cases with the same Re_τ), is generally larger for cases with higher Ri_τ values at a given y/h. This trend in FKE with respect to Ri_τ is consistent with that of the mean-flow kinetic energy [Figs. 3(a) and 3(b)]. It is important to note that the flow tends to be more energetic in cases with larger Ri_τ values under a given Re_τ before we proceed to predict intermittency. As intermittency is more likely to occur with larger Ri_τ values, FKE alone is not a reliable predictor of intermittency. This is because an intermittent flow may exhibit a higher k value than its fully turbulent counterpart, as demonstrated in Figs. 4(a) and 4(b). Essentially, Reynolds averaging serves to distinguish the energy in the fluctuations from that in the mean flow. Nevertheless, these fluctuations might also include energy from internal waves [20] or large coherent structures. This is likely why the quantity k does not precisely reflect the turbulence's energy level.
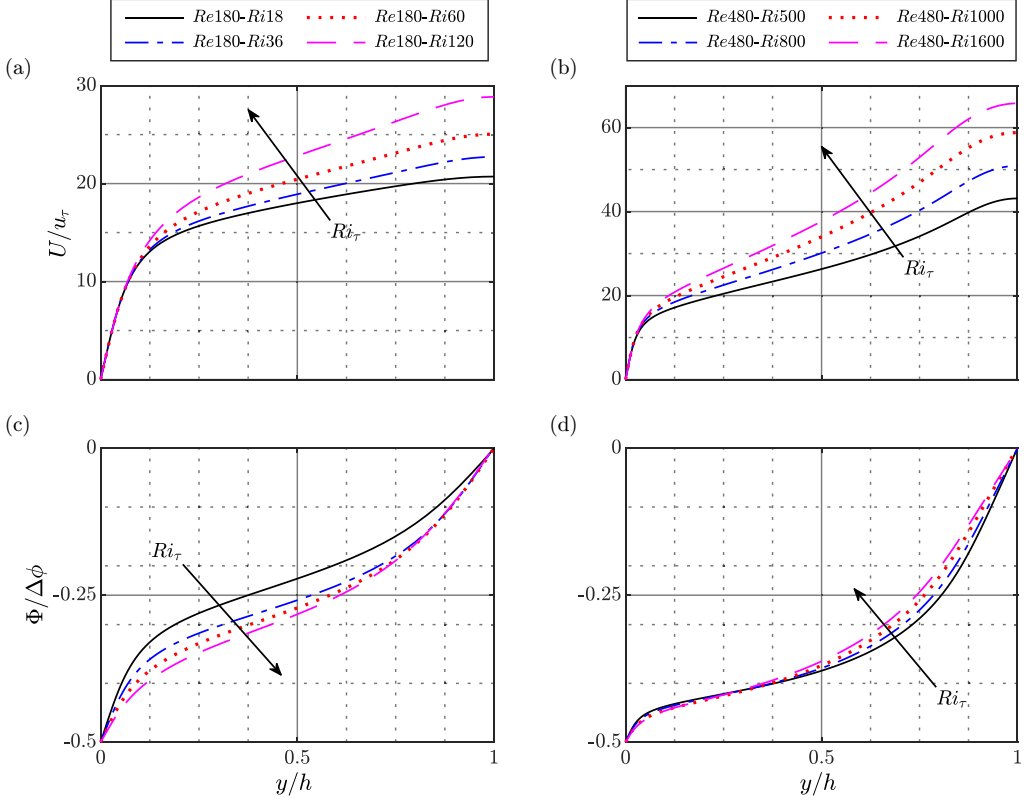
FIG. 3. Wall-normal profiles of mean velocity and potential temperature at $\mathrm{Re}_\tau = 180$ (left column) and 480 (right column) for various degrees of stratification.

The profiles of the local gradient Richardson number,

$$\mathrm{Ri}_g \equiv \frac{g\alpha_V \left(\dfrac{\partial \Phi}{\partial y} \right)}{\left(\dfrac{\partial U}{\partial y} \right)^2}, \tag{8}$$

for cases with $\mathrm{Re}_\tau = 180$ and 480 are displayed in Figs. 4(c) and 4(d). As the mean shear $\partial U/\partial y$ is zero at the midchannel due to symmetry, Ri_g approaches infinity at $y/h = 1$. In other words, there exists a highly stable region at the midchannel in SCF regardless of the Re_τ and Ri_τ values. For the lower $\mathrm{Re}_\tau = 180$ shown in Fig. 4(c), the case with a larger Ri_τ corresponds to a higher Ri_g at a given y/h, suggesting increased stability overall. However, this dependence of Ri_g on Ri_τ weakens as Re_τ increases, and the curves nearly overlap for $\mathrm{Re}_\tau = 480$ [Fig. 4(d)], where Ri_g reaches a plateau value slightly below 0.2 at $y/h \simeq 0.8$ and then increases abruptly towards the midchannel singularity at $y/h = 1$. The differences in Ri_g are insignificant among cases shown in Fig. 4(d), even though it is observed that the four cases vary from fully turbulent to intermittent (see Table I). Again, Ri_g alone would be a poor indicator for predicting intermittency, at least among the four cases considered in Fig. 4(d).
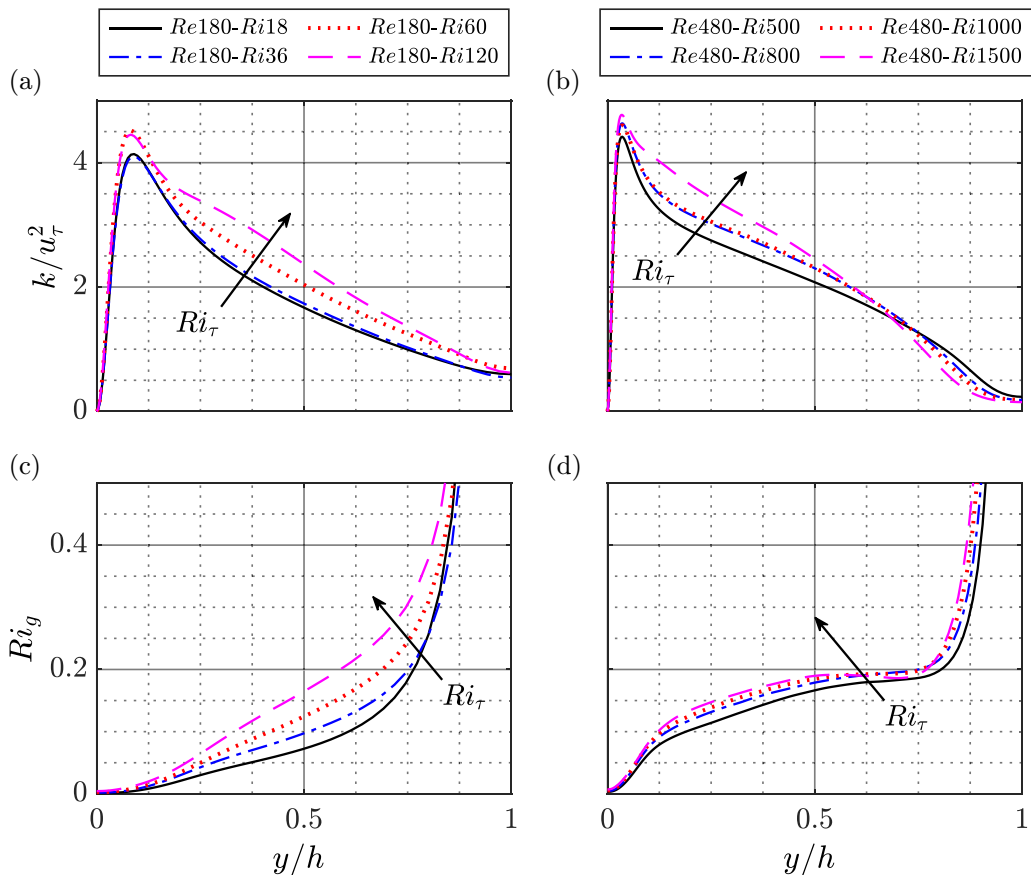
FIG. 4. Wall-normal profiles of the plane-averaged turbulent kinetic energy and gradient Richardson number at $\mathrm{Re}_\tau = 180$ (left column) and 480 (right column) for various degrees of stratification.

IV. QUANTIFYING INTERMITTENCY

A. Seperation of laminar and turbulent patches

To quantify intermittency in SCF, a dynamical marker is needed to separate laminar and turbulent regions that coexist in the flow field. There are various choices for the field variable used to identify laminar and turbulent regions, including vertical velocity magnitude [8], potential enstrophy [34] (i.e., the magnitude of potential vorticity), vertical gradient of total density [35], and magnitude of the vertical component of vorticity [36]. Following Deusebio *et al.* [10], we base our separation technique on estrophy, $\eta \equiv |\boldsymbol{\omega}|^2$, where $\boldsymbol{\omega} \equiv \nabla \times \boldsymbol{u}$ is the vorticity. At the wall the enstrophy reduces to the following form:

$$\eta_w = \left(\frac{\partial u}{\partial y}\right)^2 + \left(\frac{\partial w}{\partial y}\right)^2.$$

(9)

The local variation of η_w over a horizontal subdomain area centered around (x, z) can be quantified as follows:

$$\eta_{w,\mathrm{mbf}}(x, z) = \sqrt{\frac{1}{A} \int_{x^+, z^+} \eta_w^2 \, \mathrm{d}x^+ \, \mathrm{d}z^+ - \left[\frac{1}{A} \int_{x^+, z^+} \eta_w \, \mathrm{d}x^+ \, \mathrm{d}z^+\right]^2},$$

(10)
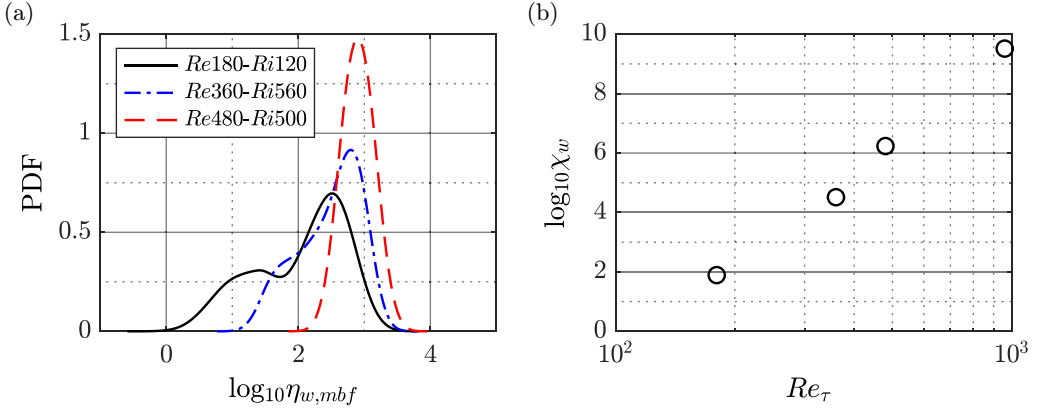
FIG. 5. (a) Examples of PDF of local variation $\eta_{w,\mathrm{mbf}}$ for typical strongly intermittent (Re180-Ri120), weakly intermittent (Re360-Ri560), and fully turbulent flows (Re480-Ri500); (b) variation of threshold χ_w against Re_τ.

where $A = \Delta x^+ \Delta z^+$ is the subdomain area, and the subscript mbf stands for "minimal box fluctuation" following Ref. [10]. The subdomain area is chosen such that it covers the size of a minimal flow unit with $\Delta x^+ \simeq 200$ and $\Delta z^+ \simeq 100$ [32]. The quantity $\eta_{w,\mathrm{mbf}}(x, z)$ is calculated for all points on the wall and provides a local measure of the fluctuation of enstrophy in the neighborhood of a given point.

The quantity $\eta_{w,\mathrm{mbf}}(x, z)$ varies strongly in space, and Fig. 5 presents examples of the probability density function (PDF) of $\eta_{w,\mathrm{mbf}}$ for cases Re180-Ri120, Re360-Ri560, and Re480-Ri500. These specific cases have been chosen because they represent strongly intermittent, weakly intermittent, and fully turbulent flows, respectively. The fully turbulent case (Re480-Ri500) produces a PDF with an approximately log-normal shape and a single prominent peak [37]. As stratification becomes more pronounced, intermittency starts to manifest, causing the PDF to skew to the left, as exemplified by the Re360-Ri560 case. For strongly intermittent cases, such as Re180-Ri120, the PDF exhibits a clear double-peak shape.

Following the approach from Ref. [10], we choose the local minimum between the two peaks, χ_w, as the threshold for differentiating between laminar and turbulent regions at the wall. For any group of cases sharing the same Re_τ, we compute the χ_w value corresponding to the case with the highest Ri_τ, and then apply this threshold value to all cases within that particular Re_τ group. Regions where $\eta_{w,\mathrm{mbf}} < \chi_w$ are classified as laminar, while those with $\eta_{w,\mathrm{mbf}} > \chi_w$ are considered turbulent. Notably, the threshold χ_w demonstrates a strong dependency on Re_τ. Figure 5(b) presents the χ_w values applied at each Re_τ, revealing an increasing trend with Re_τ. Utilizing these thresholds, the turbulent fraction at the wall, γ_w, defined as the ratio of the turbulent area to the total area, is computed for each simulation and listed in Table I. To calculate γ_w, a minimum of 20 flow snapshots, spaced approximately 0.5 advective time units (i.e., $0.5h/u_\tau$) apart, are analyzed for each case.

B. Wall-normal variation of turbulent fraction

To investigate the variations of intermittency in the wall-normal direction, we adopt the algorithm used in Ref. [10], which employed the total enstrophy, η, as the field variable to separate turbulent and laminar regions within the flow. To account for the substantial variation of enstrophy in the wall-normal direction, the threshold level, $\chi(y)$, is adjusted locally based on the local pseudo-dissipation rate, $\epsilon_K(y) \equiv \nu \langle \partial u_i'/\partial x_j \, \partial u_i'/\partial x_j \rangle$, and the corresponding dissipation at the wall, $\epsilon_{K,w}$.
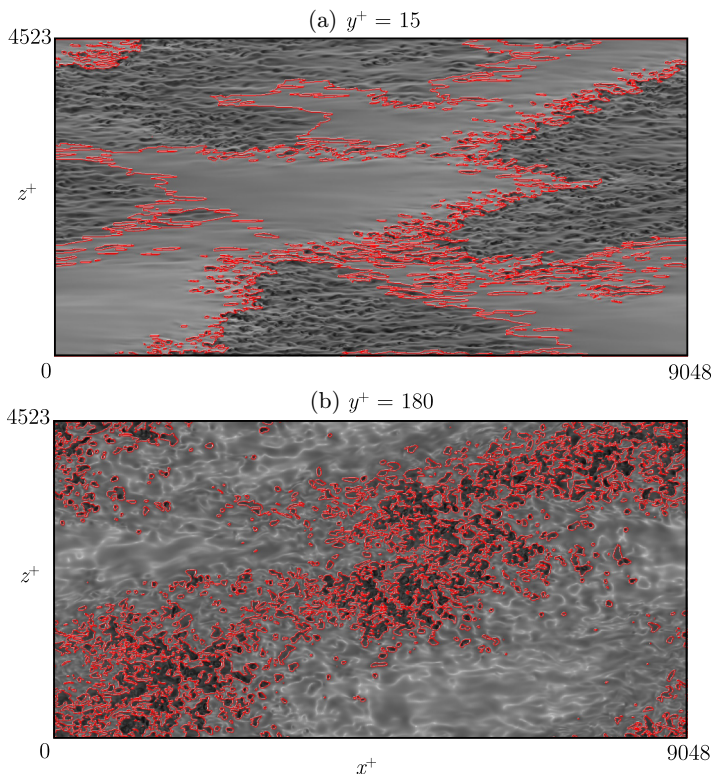
FIG. 6. Representative snapshots illustrating the identification of turbulent and nonturbulent regions using the automatic algorithm described in Ref. [10] are shown for case Re180-Ri120 at (a) $y^+ = 15$ and (b) $y^+ = 180$. The red line denotes the turbulent-nonturbulent interface and is overlaid on the enstrophy field depicted by the grayscale map.

This adjustment is performed using the following relation, similar to Ref. [10]:

$$\chi(y) = \chi_w \frac{\epsilon_K(y)}{\epsilon_{K,w}}. \tag{11}$$

Figure 6 illustrates the identification of laminar and turbulent regions in the Re180-Ri120 case. The turbulent-nonturbulent interface (indicated in red) overlays the instantaneous enstrophy field for both near-wall ($y^+ = 15$) and midchannel ($y^+ = 180$) regions. The wall-normal profile of the turbulent fraction, γ, is shown in Fig. 7. In cases with $\mathrm{Re}_\tau = 180$, γ exhibits a value smaller than unity at the wall and progressively plateaus as it moves away from the wall. This suggests that the wall may be a potential source of intermittency, unlike the open-channel flow case studied in Ref. [11] where the flow is completely turbulent at the lower wall. In stratified plane Couette flow, laminar patches are primarily confined to the wall [8], whereas in SCF an additional site of intermittency appears to emerge at the midchannel, which is reminiscent of the midchannel "blockage effect" discussed in Ref. [20]. As demonstrated in Fig. 7, cases with $\mathrm{Re}_\tau = 480$ exhibit strong intermittency at the midchannel as well, which can presumably be ascribed to the absence of shear and the consequent singularity in Ri_g (see Fig. 4). When the stratification is adequately strong, such as in the Re180-Ri120 case, the value of γ remains below unity across the entire channel, which is also illustrated in Fig. 2 (left column). This observation suggests that intermittency originating from both near-wall and midchannel regions may merge and establish a continuous connection throughout the channel's depth.
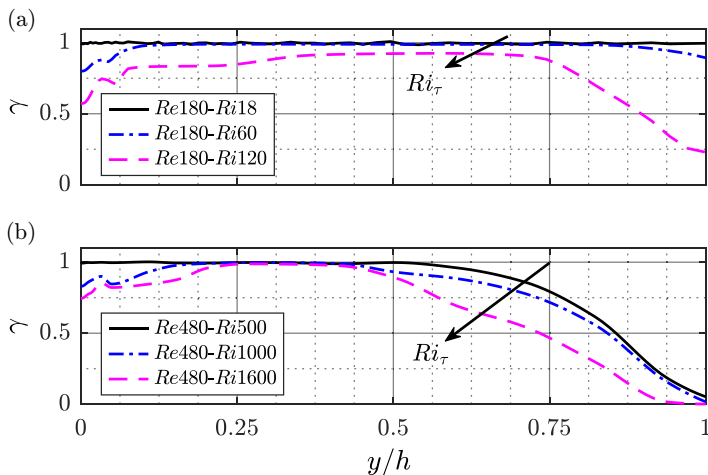
FIG. 7. Wall-normal profile of the turbulent fraction γ. Top panel: $\mathrm{Re}_\tau = 180$. Bottom panel: $\mathrm{Re}_\tau = 480$. Black, blue, and red curves represent the weakest, intermediate, and strongest degrees of stratification, respectively.

V. ONSET OF NEAR-WALL INTERMITTENCY

As discussed in Sec. I, various theories exist concerning the dynamical criterion for the onset of intermittency. The results presented in Sec. III B reveal that neither the kinetic energy level nor the gradient Richardson number (Ri_g) accurately predict this onset. In this section we continue our evaluation by examining three additional parameters, L^+, L/h, and Nu, with respect to their effectiveness in predicting the onset of near-wall intermittency (NWI), i.e., when $\gamma_w < 1.0$.

The first criterion is based on the length scale ratio between the Obukhov scale, L, defined as

$$L = \frac{u_\tau^3}{\kappa_m g \alpha_V \kappa \left(\dfrac{\partial \Phi}{\partial y} \right)_w}, \tag{12}$$

and the near-wall viscous scale, δ_v. In the above definition, k_m is the von Kármán constant ($= 0.41$). The Obukhov scale, L, approximates the height at which buoyancy effects initially become dynamically significant [38]. The ratio $L^+ \equiv L/\delta_v$ characterizes the scale separation between the height of the near-wall dynamic layer and the viscous scale of the turbulence contained within the near-wall region. Flores and Riley [7] observed the onset of intermittency for $L^+ \lesssim 100$ in numerical simulations of stratified open-channel flows, while Deusebio *et al.* [10] reported the criterion for stratified plane Couette flow to be $L^+ \lesssim 200$, attributing intermittency to a limited dynamical range of turbulent scales. Figure 8(a) illustrates the near-wall turbulent fraction γ_w plotted against L^+ for all simulations listed in Table I. The criterion $L^+ \lesssim 400$ seems to effectively identify intermittent cases, with the majority of $\gamma_w < 1$ (intermittent) instances occurring when $L^+ \lesssim 400$. However, data points from $\mathrm{Re}_\tau = 180$ appear to be outliers in Fig. 8(a), likely due to the influence of viscous effects at this low Reynolds number.

In Ref. [11] the authors utilized the locally defined $L^+ < 260$ as a criterion to predict intermittency within the interior of an open-channel flow. Notably, in their simulations, turbulence at the bottom wall consistently meets the criteria for full turbulence according to their definition, as shown in their Fig. 4(a), which depicts a turbulent fraction of 1.0 at the wall. The observation of intermittency at the wall in our SCF, in contrast to the open-channel flow investigated in Ref. [11], can be attributed in all likelihood to the different treatment of the bottom boundary. In Ref. [11] an adiabatic boundary condition was imposed at the channel bottom, inducing negligible stratification
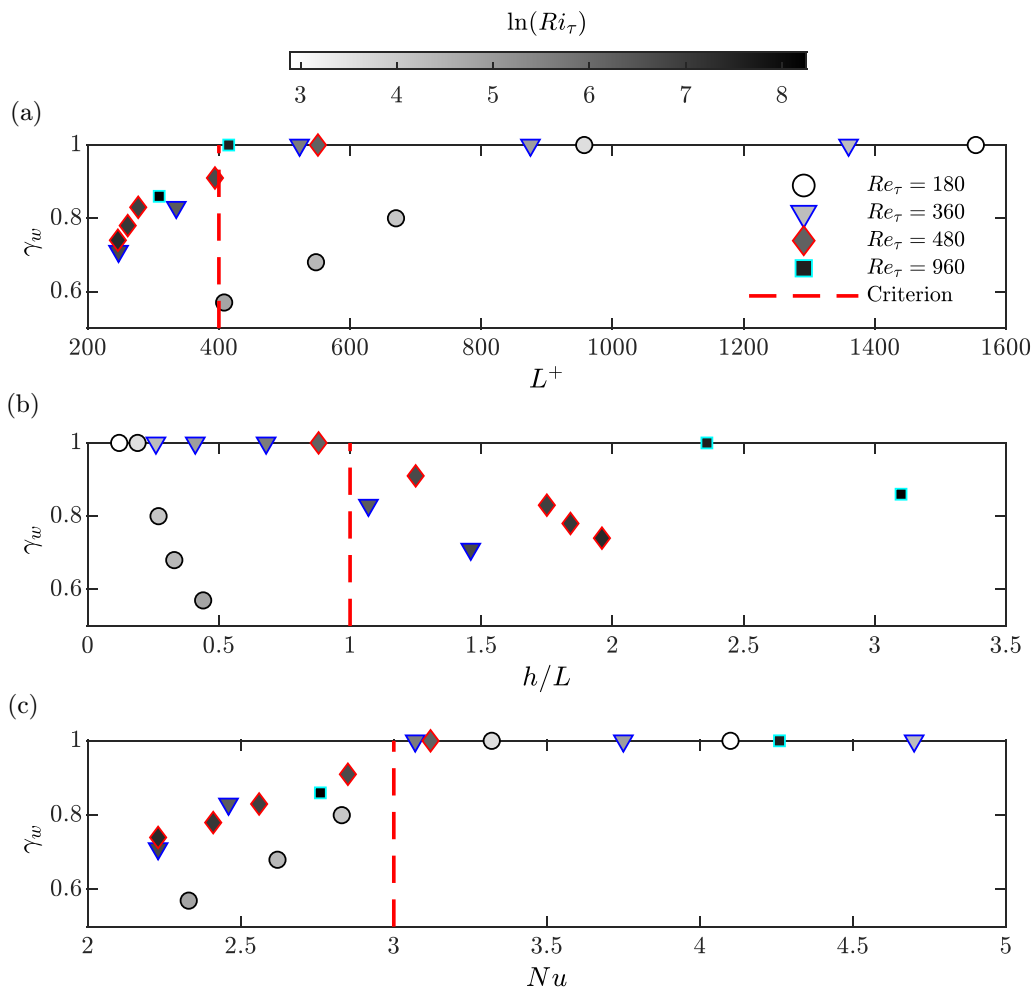
FIG. 8. Plots of γ_w with respect to three flow parameters for the entire set of simulations.

capable of suppressing turbulence. In our configuration, however, the stratification at the wall is significant (see Fig. 3), which effectively inhibits turbulence and triggers intermittency.

In the literature the stability parameter, h/L, is another criterion considered for intermittency (e.g., by Refs. [7,25,39]). Here h represents a characteristic height of the flow, which, for channel flow, is taken as the half channel height (see Fig. 1). When $h/L < 1$, buoyancy effects become dynamically insignificant throughout the entire flow. Conversely, if $h/L > 1$, stratification significantly impacts at least a portion of the flow above height L. Figure 8(b) examines the use of h/L as a criterion for the onset of NWI, comparing it to the $h/L \gtrsim 1.0$ criterion observed by Flores and Riley [7] in stratified open-channel flow. In each group with the same Re_τ, the near-wall turbulent fraction, γ_w, appears to decrease monotonically with increasing h/L. This finding aligns with the physical interpretation of this "stability" parameter, which suggests that as the flow becomes more affected by buoyancy and hence more stable, NWI is more likely to occur. However, the critical h/L value at which γ_w falls below one varies strongly with Re_τ. As Re_τ rises, the critical h/L also increases, indicating that h/L alone cannot serve as a criterion for $\gamma_w < 1.0$.

The final criterion for the onset of intermittency explored in Fig. 1(c) is based on the Nusselt number, which is simply the ratio of the wall heat flux through the turbulent flow to that of a

hypothetical, fully laminar case with a linear temperature gradient between the two walls. By definition [see Eq. (7)], a fully relaminarized channel flow would result in a Nusselt number (Nu) of unity. This led García-Villalba and del Álamo [14] to examine Nu as a criterion for flow relaminarization. They observed that at $Nu = 1.57$, the flow appears "nearly laminar."

Since we are seeking the boundary between fully turbulent flow and intermittency in the present study, the critical Nu value should naturally be larger than the relaminarization boundary examined in Ref. [14]. Deusebio *et al.* [10] attempted to use Nu as the intermittency criterion for stratified plane Couette flow and observed intermittency within a range of Nu between approximately 2 and 7 (see their Fig. 10). In the 17 stratified channel flow cases examined in this study, no intermittent cases are observed for Nu $\gtrsim 3.0$. Thus, a Nusselt number of 3.0 and above appears to be a sufficient condition for fully turbulent SCF ($\gamma_w = 1.0$), as shown in Fig. 1(c). Additionally, the γ_w vs Nu relationship for intermittent cases ($\gamma_w < 1.0$) seems to collapse nearly onto a single curve, except for the case with $Re_\tau = 180$. Out of the three potential criteria investigated in Fig. 8,

$$Nu \lesssim 3.0, \tag{13}$$

is the only one that applies to all SCF simulations examined in this study and robustly predicts the onset of near-wall intermittency. The very definition of Nu may shed some light on the Nu criterion discovered above. In turbulent flows, where convection is enhanced, the efficiency of convective heat transfer increases, leading to a higher Nu. Conversely, as the flow becomes fully laminar, heat transfer relies solely on conduction, causing Nu to approach unity. The transition to intermittency in the flow, marked by the emergence of laminar patches within turbulent regions, corresponds to a decrease in Nu from the fully turbulent state. This is because these laminar areas diminish the overall effectiveness of convective heat transfer. The Nu criterion affirms the expected behavior of Nu with the onset of intermittency and aligns well with observed data.

VI. PREDICTION OF INTERMITTENCY BOUNDARY

A. The intermittency boundary

In this section we attempt to formulate the the intermittency boundary in the Re_τ-Ri_τ plane (see a review in Ref. [40]). Specifically, we plot a contour line corresponding to Nu ≈ 3.0 within the parameter space to represent the intermittency boundary, as indicated by the dashed-dotted line in Fig. 9. This line for Nu ≈ 3.0 was obtained by applying a Reynolds-averaged Navier-Stokes (RANS) model for many combinations of (Re_τ, Ri_τ). Details on this RANS model can be found in the Appendix. The relaminarization boundary based on stability analysis, as described by Ref. [22], is depicted by a solid line in Fig. 9. The symbols represent four groups of simulations with varying Re_τ values. These symbols are filled using a grayscale that corresponds to the near-wall turbulent fraction, γ_w, with darker shades representing a larger γ_w. Several key observations can be made from Fig. 9:

(1) At a given Re_τ, the flow transitions from a fully turbulent state (represented by fully dark symbols) to an intermittent state (depicted by gray symbols), and ultimately to a laminar state as stratification increases, i.e., with an increased value of Ri_τ.

(2) As Re_τ increases by nearly one order of magnitude from 180 to 960, the critical Ri_τ at which the onset of intermittency occurs is reached at a considerably larger value.

(3) The intermittency boundary, denoted by a dash-dotted line, exhibits an approximate power law of $Ri_\tau \propto Re_\tau^2$, a scaling we explore further in the next subsection. The boundary's slope of 2, while generally reliable for larger Re_τ values, shows less accuracy at $Re_\tau = 180$. Specifically, the data point $(Re_\tau, Ri_\tau) = (180, 60)$ is classified as fully turbulent according to the boundary depicted in Fig. 9. However, DNS data indicate that this flow is actually intermittent, with $\gamma_w = 0.83$. This discrepancy arises because the RANS model used to predict the boundary tends to overestimate Nu for this Re_τ value, as shown in Fig. 12 in the Appendix. Apart from this particular case at the lowest examined Re_τ value, the intermittency boundary with a slope of 2 aligns well with the rest of the
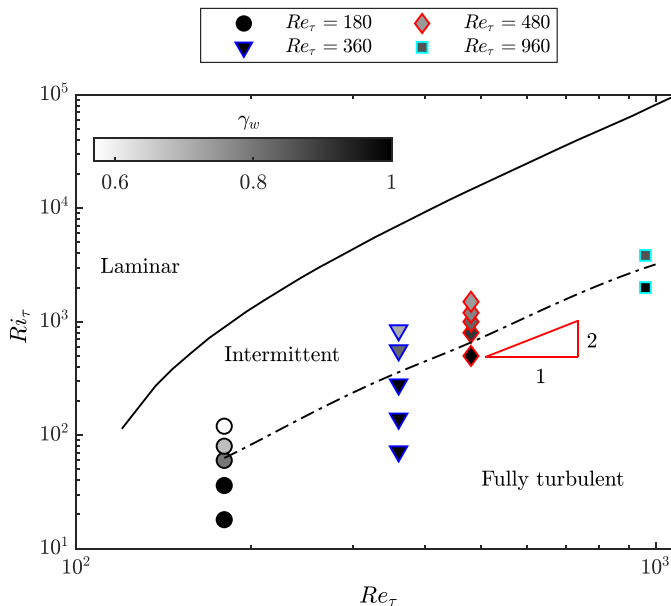
FIG. 9. Diagram showing various flow regimes in the Re_τ-Ri_τ plane, including the relaminarization boundary (solid line) based on linear stability analysis [22], the intermittency boundary (dash-dotted line) derived from the RANS model, and a compilation of DNS data (circles) color-coded by the wall turbulent fraction, γ_w. The hypotenuse of the red triangle denotes a power-law slope of $Ri_\tau \propto Re_\tau^2$.

DNS data. Due to the aforementioned issues of the RANS model, caution should be exercised when considering the predicted boundary at lowest value of Re_τ at 180.

B. The $Ri_\tau \propto Re_\tau^2$ scaling

The dashed-dotted line in Fig. 9 delineates the intermittency boundary, representing the combination of Re_τ and Ri_τ that gives rise to a Nusselt number (Nu) of approximately 3.0. In a recent DNS study by Zonta *et al.* [20], a scaling relationship is provided as follows:

$$NuRe_\tau^{-2/3} \propto Ri_\tau^{-1/3}, \tag{14}$$

which aligns well with existing numerical data (see Fig. 14 in Ref. [20]). We corroborate this scaling using our own DNS results in Fig. 10 and find a notable consistency. Furthermore, our data provide a fitting result expressed as $NuRe_\tau^{-2/3} \approx 0.36Ri_\tau^{-1/3}$, which is represented by the dashed line in Fig. 10. By considering the condition Nu ≈ 3.0 for intermittency onset, we derive

$$Re_\tau Ri_\tau^{-1/2} = \text{const} \approx 24, \tag{15}$$

which can be identified as the intermittency boundary. The above scaling is substantiated by Fig. 9, where the intermittency boundary determined via the RANS model exhibits a power-law slope of $Ri_\tau \propto Re_\tau^2$, particularly at $Re_\tau > 180$, affirming the analysis that led to Eq. (15).

VII. CONCLUDING REMARKS

In this work we have investigated wall-bounded turbulence in stratified channel flow using direct numerical simulations (Sec. II), with the aim of understanding both qualitative (Sec. III) and quantitative (Sec. IV) characteristics and predicting the occurrence of global intermittency in SCF (Secs. V and VI). We have explored the flow dynamics over a range of Ri_τ values for Re_τ
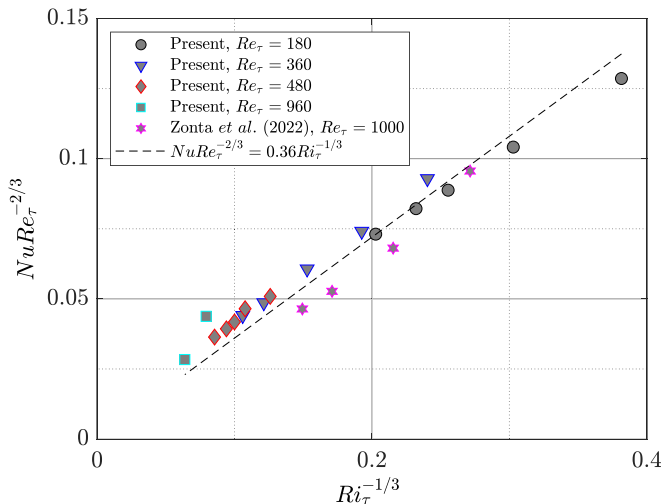
FIG. 10. $NuRe_\tau^{-2/3}$ as a function of the friction Richardson number $Ri_\tau^{-1/3}$. Results of present study are shown together with those obtained in Ref. [20].

ranging from 180 to 960 (Table I), covering both intermittent and fully turbulent regimes in SCF. We have observed two potential sites of intermittency (Fig. 7), one near the wall and the other at midchannel. We have particularly focused on near-wall intermittency and identified the Nusselt number (Nu) as the parameter dictating the onset of NWI (Fig. 8). To predict the onset of NWI in the parameter space, we have developed a first-order closure model (see the Appendix) that reliably predicts Nu as a function of Re_τ and Ri_τ (Fig. 12). All these results have led to the delineation of the intermittency boundary shown in Fig. 9, which suggests that, for the range of parameters investigated, the transition from fully turbulent to intermittent states occurs at $Re_\tau Ri_\tau^{-1/2} = $ const in the parameter space, i.e., Eq. (15).

Our findings for the SCF reveal a significant dynamical distinction between a constant-flux layer, exemplified by a stratified plane Couette flow [10], and the SCF, where both momentum and buoyancy fluxes display complex variations in the wall-normal direction. In the case of the constant-flux layer scenario, Deusebio et al. [10] identified a criterion of $L^+ \lesssim 200$ for the onset of intermittency. However, for the SCF, as illustrated in Fig. 8(a), the criterion appears to be $L^+ \lesssim 400$ for $Re_\tau \geqslant 360$, with an even higher L^+ threshold for $Re_\tau = 180$. Conversely, we determined that Nu $\lesssim 3.0$ offers a reliable criterion for near-wall intermittency in the SCF [Fig. 8(c)], while for the Couette flow, no clear cutoff Nu value for intermittency seems to exist (see Fig. 10 of Ref. [10]). In the context of stably stratified atmospheric boundary layer flows (e.g., see a review by Mahrt [2]), neither the SCF nor a constant-flux layer can adequately capture the intricate structures within these flows. Consequently, the intermittency criteria derived from idealized configurations should be applied cautiously in atmospheric flow scenarios. In our setup, absent of time-varying submeso-scale forcing, we indeed observe intermittency, hinting at the possibility that intermittency is an inherent characteristic of stratified turbulence near the wall, rather than being forced exclusively by submeso-scale motions [2].

A practical challenge in conducting DNS studies of stratified turbulence is to access large Reynolds numbers, which demand substantial computational resources. In this study the highest Re_τ achieved is 960, comparable to a recent DNS of SCF [20] that examined $Re_\tau = 1000$. Although Ri_τ increases monotonically with Re_τ for the intermittency boundary identified at $Re_\tau \leqslant 960$ (as depicted in Fig. 9), it remains uncertain whether the $Ri_\tau \propto Re_\tau^2$ scaling holds for flows with larger Re_τ values than those investigated here. Specifically, will the intermittency boundary level off as $Re_\tau \to \infty$, or will the critical Ri_τ also approach infinity following the same power law?

Intermittency is a widespread phenomenon in stratified flows, many of which are not directly influenced by wall effects, such as homogenous turbulence (e.g., Ref. [35]) or strongly stratified wakes (e.g., Refs. [41,42]). Consequently, an intriguing direction for future research would be to determine the intermittency boundary for these non-wall-bounded stratified flows, in which neither the Nu nor the L^+ criterion is applicable. The complex interactions between internal waves and intermittency could be significant in geophysical flows. One challenge in this line of inquiry is how to separate contributions from internal waves or other coherent structures from the small-scale turbulence; a possible solution to this is employing the triple decomposition methodology, which has been successful for several canonical flows [43,44]. To thoroughly investigate these dynamics, larger horizontal domains than those employed in this study are recommended. This is due to the considerable length scales associated with internal waves, as discussed in the literature (see e.g., Zonta *et al.* [20]).

APPENDIX: REYNOLDS-AVERAGED NAVIER-STOKES MODEL

The Nusselt number criterion (13) for the onset of intermittency, shown in Sec. VI, can be utilized to determine the intermittency boundary on the Re_τ-Ri_τ plane. This helps in predicting the onset of global intermittency in SCF as a function of the control parameters. For this purpose, it is crucial to develop a model that estimates the Nusselt number based on Re_τ and Ri_τ. In this Appendix we present a RANS model specifically formulated for this task.

The Reynolds-averaged momentum (U) and buoyancy (Φ) equations for SCF are as follows:

$$\frac{\partial U}{\partial t} = \nu \frac{\partial^2 U}{\partial y^2} + \frac{u_\tau^2}{h} - \frac{\partial \langle u'v' \rangle}{\partial y}, \tag{A1a}$$

$$\frac{\partial \Phi}{\partial t} = \kappa \frac{\partial^2 \Phi}{\partial y^2} - \frac{\partial \langle v'\phi' \rangle}{\partial y}. \tag{A1b}$$

These equations are solved numerically to obtain the steady-state solution for U and Φ. In the RANS model, the Reynolds stress and buoyancy flux terms are represented by the turbulent viscosity (ν_t) and diffusivity (κ_t) multiplied by the respective mean gradients:

$$-\langle u'v' \rangle = \nu_t \frac{\partial U}{\partial y}, \tag{A2a}$$

$$-\langle v'\phi' \rangle = \kappa_t \frac{\partial \Phi}{\partial y}. \tag{A2b}$$

Subsequently, a closure model for ν_t and κ_t is required. A popular first-order scheme for stable boundary layers is one proposed by Brost and Wyngaard [45]. This parametrization has proven effective in operational weather and climate models (see, e.g., Refs. [46–49]). In Ref. [45] the eddy
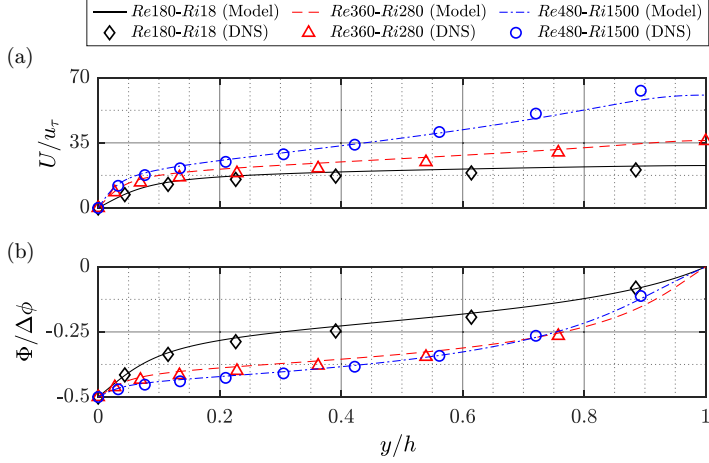
FIG. 11. Comparison of predicted mean profiles for streamwise velocity (U) and potential temperature (Φ) with DNS data. Results for cases Re180-Ri18, Re360-Ri280, and Re480-Ri1500 are shown as examples.

viscosity is given by

$$\nu_t = k_m u_\tau \hat{y} \frac{\left(1 - \dfrac{\hat{y}}{H}\right)^{1.5}}{1 + 4.7\dfrac{\hat{y}}{L}}, \tag{A3}$$

where $\hat{y}$ is the wall-normal distance, and H represents the characteristic depth of the stable boundary layer (SBL) and must be parameterized.

Current research is inconclusive regarding the parametrization of SBL height H, a question that is complicated by complex forcings in atmospheric boundary layers (see, e.g., Refs. [50–54]). Given that the gradient Richardson number increases monotonically with wall-normal distance, as illustrated in Fig. 4, it is convenient to base the estimate of SBL depth H on Ri_g. Specifically, one can identify H by finding the wall-normal distance $\hat{y}$ such that Ri_g retains the critical value $\mathrm{Ri}_{g,c}$, i.e., $\mathrm{Ri}_g|_{\hat{y}=H} = \mathrm{Ri}_{g,c}$. It follows that for height $\hat{y} > H$, the flow is "stable" with $\mathrm{Ri}_g > \mathrm{Ri}_{g,c}$, and vice versa. This definition is employed to estimate H dynamically during the RANS calculation. Multiple choices for the numerical values of $\mathrm{Ri}_{g,c}$ exist (see Table I of Ref. [53]), and a value of 0.25 is adopted in our model following the Miles-Howard criterion.

As suggested by our DNS data (not shown), the turbulent Prandtl number, i.e., the ratio of the turbulent viscosity to the turbulent diffusivtity, ν_t/κ_t, is close to unity for the entire channel except in regions within close proximity to the wall. We thus set $\nu_t = \kappa_t$ in the RANS model. In the near-wall region, the values of ν_t and κ_t are corrected using the van Driest damping function to ensure their correct convergence rate toward the wall [19,55].

Figure 11 illustrates the wall-normal profiles of streamwise velocity and potential temperature predicted by the first-order closure model. The model demonstrates good agreement with DNS data, accurately reproducing the profiles in both intermittent and fully turbulent flow states.

In Sec. V our analysis suggests that the onset of intermittency for SCF occurs at Nu ≈ 3.0. To evaluate the model's accuracy in predicting Nu, we apply it to calculate Nu for all cases included in our DNS runs, as well as data provided in Refs. [14,20]. Figure 12 displays the Nu predicted by the RANS model, alongside the DNS data for comparison. The predicted values generally show good agreement with DNS, although it should be noted that the relative errors tend to be larger for cases with the lowest friction Reynolds number ($\mathrm{Re}_\tau = 180$), and that the model seems to consistently
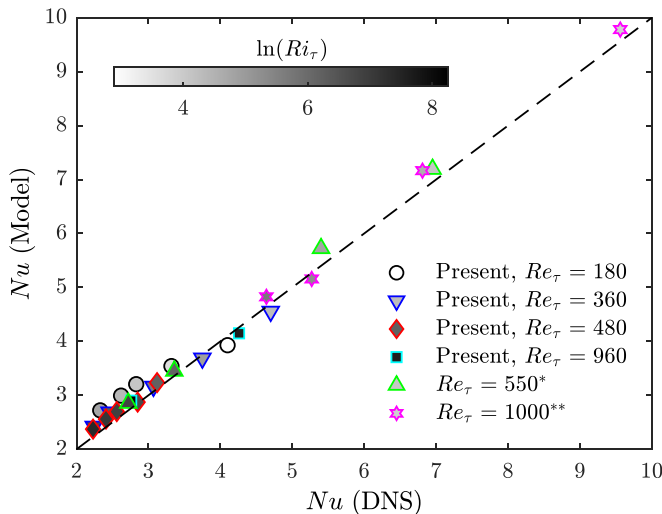
FIG. 12. Comparison of Nusselt number between the model and DNS. The symbols are color-coded with the natural logarithm of Ri_τ. DNS data for $Re_\tau = 550$ are from Ref. [14], and for $Re_\tau = 1000$ from Ref. [20].

overestimate Nu as compared to DNS results. However, the model's overall performance is deemed acceptable, as the relative error between model-predicted values and DNS data stays within 10%.

[1] L. Mahrt, Intermittency of atmospheric turbulence, J. Atmos. Sci. **46**, 79 (1989).

[2] L. Mahrt, Stably stratified atmospheric boundary layers, Annu. Rev. Fluid Mech. **46**, 23 (2014).

[3] S. M. de Bruyn Kops, Classical scaling and intermittency in strongly stratified Boussinesq turbulence, J. Fluid Mech. **775**, 436 (2015).

[4] F. T. M. Nieuwstadt, The turbulent structure of the stable, nocturnal boundary layer, J. Atmos. Sci. **41**, 2202 (1984).

[5] L. Mahrt, Stratified atmospheric boundary layers, Boundary Layer Meteorol. **90**, 375 (1999).

[6] B. J. H. van de Wiel, A. F. Moene, R. J. Ronda, H. A. R. De Bruin, and A. A. M. Holtslag, Intermittent turbulence and oscillations in the stable boundary layer over land. Part II: A system dynamics approach, J. Atmos. Sci. **59**, 2567 (2002).

[7] O. Flores and J. J. Riley, Analysis of turbulence collapse in the stably stratified surface layer using direct numerical simulation, Boundary Layer Meteorol. **139**, 241 (2011).

[8] G. Brethouwer, Y. Duguet, and P. Schlatter, Turbulent-laminar coexistence in wall flows with Coriolis, buoyancy or Lorentz forces, J. Fluid Mech. **704**, 137 (2012).

[9] C. Ansorge and J. P. Mellado, Global intermittency and collapsing turbulence in the stratified planetary boundary layer, Boundary Layer Meteorol. **153**, 89 (2014).

[10] E. Deusebio, C. P. Caulfield, and J. R. Taylor, The intermittency boundary in stratified plane Couette flow, J. Fluid Mech. **781**, 298 (2015).

[11] V. Issaev, N. Williamson, and S. W. Armfield, Intermittency and critical mixing in internally heated stratified channel flow, J. Fluid Mech. **963**, A5 (2023).

[12] A. Prigent, G. Grégoire, H. Chaté, O. Dauchot, and W. van Saarloos, Large-scale finite-wavelength modulation within turbulent shear flows, Phys. Rev. Lett. **89**, 014501 (2002).

[13] Q. Zhou, J. R. Taylor, and C. P. Caulfield, Self-similar mixing in stratified plane Couette flow for varying Prandtl number, J. Fluid Mech. **820**, 86 (2017).

[14] M. García-Villalba and J. C. del Álamo, Turbulence modification by stable stratification in channel flow, Phys. Fluids **23**, 045104 (2011).

[15] R. P. Garg, J. H. Ferziger, S. G. Monismith, and J. R. Koseff, Stably stratified turbulent channel flows. I. Stratification regimes and turbulence suppression mechanism, Phys. Fluids **12**, 2569 (2000).

[16] V. Armenio and S. Sarkar, An investigation of stably stratified turbulent channel flow using large-eddy simulation, J. Fluid Mech. **459**, 1 (2002).

[17] O. Iida, N. Kasagi, and Y. Nagano, Direct numerical simulation of turbulent channel flow under stable density stratification, Int. J. Heat Mass Transfer **45**, 1693 (2002).

[18] H. Cen, Q. Zhou, and A. Korobenko, Simulation of stably stratified turbulent channel flow using residual-based variational multiscale method and isogeometric analysis, Comput. Fluids **214**, 104765 (2021).

[19] H. Cen, Q. Zhou, and A. Korobenko, Wall-function-based weak imposition of Dirichlet boundary condition for stratified turbulent flows, Comput. Fluids **234**, 105257 (2022).

[20] F. Zonta, P. H. Sichani, and A. Soldati, Interaction between thermal stratification and turbulence in channel flow, J. Fluid Mech. **945**, A3 (2022).

[21] H. Cen, Modeling and analysis of stably stratified wall-bounded turbulent flows, Ph.D. dissertation, University of Calgary, 2022.

[22] K. S. Gage and W. H. Reid, The stability of plane Poiseuille flow, J. Fluid Mech. **33**, 21 (1968).

[23] J. W. Miles, On the stability of heterogeneous shear flows, J. Fluid Mech. **10**, 496 (1961).

[24] L. N. Howard, Note on a paper of John W. Miles, J. Fluid Mech. **10**, 509 (1961).

[25] F. T. M. Nieuwstadt, Direct numerical simulation of stable channel flow at large stability, Boundary Layer Meteorol. **116**, 277 (2005).

[26] J. R. Taylor, S. Sarkar, and V. Armenio, Large eddy simulation of stably stratified open channel flow, Phys. Fluids **17**, 116602 (2005).

[27] A. Atoufi, K. A. Scott, and M. L. Waite, Characteristics of quasistationary near-wall turbulence subjected to strong stable stratification in open-channel flows, Phys. Rev. Fluids **5**, 064603 (2020).

[28] J. R. Taylor, Numerical simulations of the stratified oceanic bottom boundary layer, Ph.D. dissertation, University of California, San Diego, 2008.

[29] Q. Zhou, J. R. Taylor, C. P. Caulfield, and P. F. Linden, Diapycnal mixing in layered stratified plane Couette flow quantified in a tracer-based coordinate, J. Fluid Mech. **823**, 198 (2017).

[30] C. Canuto, M. Y. Hussaini, A. Quarteroni, and T. A. Zang, Jr, *Spectral Methods in Fluid Dynamics* (Springer, Berlin, 1988).

[31] P. Moin and K. Mahesh, Direct numerical simulation: A tool in turbulence research, Annu. Rev. Fluid Mech. **30**, 539 (1998).

[32] J. Jiménez and P. Moin, The minimal flow unit in near-wall turbulence, J. Fluid Mech. **225**, 213 (1991).

[33] O. Flores and J. Jiménez, Hierarchy of minimal flow units in the logarithmic layer, Phys. Fluids **22**, 071704 (2010).

[34] T. Watanabe, J. J. Riley, S. M. de Bruyn Kops, P. J. Diamessis, and Q. Zhou, Turbulent/non-turbulent interfaces in wakes in stably stratified fluids, J. Fluid Mech. **797**, R1 (2016).

[35] G. D. Portwood, S. M. de Bruyn Kops, J. R. Taylor, H. Salehipour, and C. P. Caulfield, Robust identification of dynamically distinct regions in stratified turbulence, J. Fluid Mech. **807**, R2 (2016).

[36] B. Halawa, S. Merhi, C. Tang, and Q. Zhou, Three-dimensional visualization of stratified turbulent wakes at varying Reynolds number, J. Visualization **23**, 437 (2020).

[37] R. Örlü and P. Schlatter, On the fluctuating wall-shear stress in zero pressure-gradient turbulent boundary layer flows, Phys. Fluids **23**, 021704 (2011).

[38] J. C. Wyngaard, *Turbulence in the Atmosphere* (Cambridge University Press, Cambridge, 2010).

[39] B. J. H. Van De Wiel, A. F. Moene, G. J. Steeneveld, O. K. Hartogensis, and A. A. M. Holtslag, Predicting the collapse of turbulence in stably stratified boundary layers, Flow Turbul. Combust. **79**, 251 (2007).

[40] F. Zonta and A. Soldati, Stably stratified wall-bounded turbulence, Appl. Mech. Rev. **70**, 040801 (2018).

[41] Q. Zhou and P. J. Diamessis, Large-scale characteristics of stratified wake turbulence at varying Reynolds number, Phys. Rev. Fluids **4**, 084802 (2019).

[42] Q. Zhou, Threshold behavior of local gradient Richardson number in strongly stratified nonequilibrium turbulence, Phys. Rev. Fluids **7**, 104802 (2022).

[43] W. C. Reynolds and A. K. M. F. Hussain, The mechanics of an organized wave in turbulent shear flow. Part 3. Theoretical models and comparisons with experiments, J. Fluid Mech. **54**, 263 (1972).

[44] A. Soldati and S. Banerjee, Turbulence modification by large-scale organized electrohydrodynamic flows, Phys. Fluids **10**, 1742 (1998).

[45] R. A. Brost and J. C. Wyngaard, A model study of the stably stratified planetary boundary layer, J. Atmos. Sci. **35**, 1427 (1978).

[46] J. F. Louis, A parametric model of vertical eddy fluxes in the atmosphere, Boundary Layer Meteorol. **17**, 187 (1979).

[47] A. C. M. Beljaars and A. A. M. Holtslag, Flux parameterization over land surfaces for atmospheric models, J. Appl. Meteorol. **30**, 327 (1991).

[48] Y. Noh, W. G. Cheon, S. Y. Hong, and S. Raasch, Improvement of the K-profile model for the planetary boundary layer based on large eddy simulation data, Boundary Layer Meteorol. **107**, 401 (2003).

[49] J. E. Pleim, A combined local and nonlocal closure model for the atmospheric boundary layer. Part I: Model description and testing, J. Appl. Meteorol. Climatol. **46**, 1383 (2007).

[50] A. A. M. Holtslag and F. T. M. Nieuwstadt, Scaling the atmospheric boundary layer, Boundary Layer Meteorol. **36**, 201 (1986).

[51] D. H. P. Vogelezang and A. A. M. Holtslag, Evaluation and model impacts of alternative boundary-layer height formulations, Boundary Layer Meteorol. **81**, 245 (1996).

[52] B. Kosović and J. A. Curry, A large eddy simulation study of a quasi-steady, stably stratified atmospheric boundary layer, J. Atmos. Sci. **57**, 1052 (2000).

[53] S. Zilitinkevich and A. Baklanov, Calculation of the height of the stable boundary layer in practical applications, Boundary Layer Meteorol. **105**, 389 (2002).

[54] D. Vickers and L. Mahrt, Evaluating formulations of stable boundary layer height, J. Appl. Meteorol. **43**, 1736 (2004).

[55] S. B. Pope, *Turbulent Flows* (Cambridge University Press, Cambridge, 2000).